1-D Lamination Models for Calculating the Magnetization Dynamics in Non-Oriented Soft Magnetic Steel Sheets

M. Petrun,[1] S. Steentjes,[2] K. Hameyer,[2] and D. Dolinar[1]

[1]Institute of Power Engineering, University of Maribor, Maribor SI-2000, Slovenia
[2]Institute of Electrical Machines, RWTH Aachen University, Aachen D-52062, Germany

This paper presents 1-D dynamic magnetization models of non-oriented soft magnetic steel sheets that can be expressed as simple systems of ordinary differential equations. The discussed models take into account the dynamic effects on magnetization due to eddy currents and hysteresis inside such sheets and differ in the way the coupled Maxwell equations with hysteresis are solved. The presented modeling approaches include finite-difference schemes of different accuracies, various magnetic equivalent circuits (MECs), including a recent approach to eliminate the deficiencies of classical MECs, and a mesh-free approach. The different modeling approaches are analyzed and compared in terms of mathematical structure, implementation work, spatial discretization, and accuracy, where both voltage- and current-driven versions are investigated.

Index Terms— **Dynamic modeling, eddy currents, finite differences (FDs), flux tube, magnetic hysteresis, mesh-free (MF) eddy-current model.**

I. Introduction

THE dynamic behavior of ferromagnetic cores operating under distorted flux waveforms is the result of several intertwined phenomena: 1) eddy currents, 2) skin effect, 3) saturation, and 4) hysteresis. The substantial interaction between hysteresis and eddy currents cannot be solved without a strongly coupled model. The quantitative description of the magnetization process in a thin long sheet when neglecting edge effects is reduced to the integration of a 1-D penetration equation that links the magnitudes of the magnetic field strength H, the magnetic flux density B, and the electric field strength E within a material with specific electrical conductivity σ and a non-linear, hysteretic relation $B(H)$.

First, numerical solutions to the penetration equation were obtained using the finite-difference (FD) method using compact or non-compact stencils [1]–[3]. Then, the finite-element (FE) method allowed for considering the distributive nature of the time derivative over some spatial domain [3]–[5]. The analysis in [3] revealed that it is unnecessary to use the FE method in the case of the simple boundary conditions of a thin sheet. FD schemes with time derivatives distributed over three and five neighboring nodes can be deduced, comparing well to the FE schemes using quadratic and cubic interpolation functions, respectively [2].

In addition, magnetic equivalent circuit (MEC) approaches were proposed, which are based on the definitions of electric and magnetic flux tubes, for building a network to compute electrical (resistance) and magnetic (reluctance) lumped parameters [4]. Similarly, the magnetic field and eddy-current distributions inside a lamination can be solved using the parametric magneto-dynamic model (PMD) [8], [9], where the diffusion phenomena are effectively solved based on a simple matrix differential equation.

As an alternative, simplifying mesh-free (MF) approaches like the ones in [6] and [7] were also proposed, which approximate the magnetic flux density distribution in the lamination depth by a set of orthogonal basis functions, allowing an efficient coupling to FE simulations.

The discussed 1-D soft magnetic steel sheet (SMSS) models differ in the ways the coupled problems are solved. However, all the discussed models can be expressed as simple systems of ordinary differential equations (ODEs) and are coupled to a static hysteresis model, e.g., the Jiles–Atherton model [10]. In this paper, the coupled models are finally compared in terms of mathematical structure, implementation, computational performance, accuracy, and spatial discretization, where both the voltage- and current-driven versions are evaluated.

II. Theoretical Background

Measured quantities in Epstein frames or single-sheet testers are the currents and fluxes related to the magnetic field at the surface of the lamination and the average magnetic flux density across the lamination thickness. Symmetries of the measurement tools and the geometry of the sample facilitate working with a 1-D formulation of the problem

$$\sigma \frac{\partial B}{\partial t} = \frac{\partial^2 H}{\partial z^2}. \tag{1}$$

Considering a lamination of thickness d with an upper surface normal vector $\mathbf{n} = (0, 0, 1)$, the domain of analysis is a line parallel to $\mathbf{n}$, across half the thickness $[0, d/2]$. Various methods for solving the coupled problem are briefly explained in Sections II-A–D, where the constitutive relationship $B(H)$ is realized through a static hysteresis model.

A. Finite-Differences Modeling Approach

The simplest FD-scheme for solving (1) is a second-order scheme based on central difference approximation [1]–[3], linking the magnetic fields and flux densities of the internal

Manuscript received July 6, 2015; revised August 25, 2015 and August 31, 2015; accepted September 15, 2015. Date of publication September 22, 2015; date of current version February 17, 2016. Corresponding authors: M. Petrun (e-mail: martin.petrun@um.si) and S. Steentjes (e-mail: simon.steentjes@iem.rwth-aachen.de).

Color versions of one or more of the figures in this paper are available online at http://ieeexplore.ieee.org.

Digital Object Identifier 10.1109/TMAG.2015.2480416

nodes of the FD-grid along the line

$$\frac{\mathrm{d}B_\mathrm{i}}{\mathrm{d}t} = \frac{H_{\mathrm{i}-1} - 2H_\mathrm{i} + H_{\mathrm{i}+1}}{\sigma h^2}. \tag{2}$$

Here $H_\mathrm{i}(t) = H(z_\mathrm{i}, t)$ and $B_\mathrm{i}(t) = B(z_\mathrm{i}, t)$ are the sought grid functions corresponding to the node i, where $h = d/(2(N-1))$ is the grid spacing related to N uniformly distributed nodes [2]. Using the semi-discrete form of (2) reduces the boundary value problem (BVP) for the magnetic circuit to an initial value problem for ODEs [2], being further on compatible with the ODEs of an external electrical circuit. Based on (2) with the prescribed Neumann BVP, the voltage-driven second-order FD-scheme (3) is obtained

$$\frac{\mathrm{d}B_1}{\mathrm{d}t} = \frac{8H_2 - 7H_1 - H_3}{2\sigma h^2} + \frac{3(N-1)}{n_\mathrm{p} A_\mathrm{Fe}} u_\mathrm{ind}(t) \tag{3a}$$

$$\frac{\mathrm{d}B_\mathrm{i}}{\mathrm{d}t} = \frac{H_{\mathrm{i}-1} - 2H_\mathrm{i} + H_{\mathrm{i}+1}}{\sigma h^2} \quad \forall i = 2, \ldots, N-1 \tag{3b}$$

$$\frac{\mathrm{d}B_\mathrm{N}}{\mathrm{d}t} = \frac{2(H_{\mathrm{N}-1} - H_\mathrm{N})}{\sigma h^2} \tag{3c}$$

where the induced magnetization voltage u_ind or the space-averaged magnetic flux density B_a is a prescribed function of time, n_p is the number of turns of the excitation winding, and A_Fe is the cross section of the SMSS. In the current-driven version, i.e., when the magnetization current $i_\mathrm{p}(t)$ is a given function of time, a Dirichlet BVP is obtained and the magnetic field strength H_1 at the surface of the sheet is impressed, thus omitting (3a). These second-order schemes are called voltage- or current-driven FD-h^2 in the following.

In addition, FD schemes with accuracy $O(h^4)$ (called FD-h^4) that have distributed time derivatives over three nodes are applied. FD-h^4 schemes are obtained starting from the Taylor expansion of the magnetic field $H_{\mathrm{i}\pm1}$ using centered differences to eliminate the fourth derivative [3]

$$\frac{97}{30}\frac{\mathrm{d}B_1}{\mathrm{d}t} + \frac{19}{5}\frac{\mathrm{d}B_2}{\mathrm{d}t} - \frac{13}{10}\frac{\mathrm{d}B_3}{\mathrm{d}t} + \frac{4}{15}\frac{\mathrm{d}B_4}{\mathrm{d}t} = 12\frac{H_2 - H_1}{\sigma h^2} + \frac{12(N-1)}{n_1 A_\mathrm{Fe}} u_\mathrm{ind}(t) \tag{4a}$$

$$\frac{\mathrm{d}B_{\mathrm{i}-1}}{\mathrm{d}t} + 10\frac{\mathrm{d}B_\mathrm{i}}{\mathrm{d}t} + \frac{\mathrm{d}B_{\mathrm{i}+1}}{\mathrm{d}t} = \frac{12(H_{\mathrm{i}-1} - 2H_\mathrm{i} + H_{\mathrm{i}+1})}{\sigma h^2} \tag{4b}$$

$$\frac{\mathrm{d}B_{\mathrm{N}-1}}{\mathrm{d}t} + 5\frac{\mathrm{d}B_\mathrm{N}}{\mathrm{d}t} = 12\frac{(H_{\mathrm{N}-1} - H_\mathrm{N})}{\sigma h^2}. \tag{4c}$$

B. Mesh-Free Modeling Approach

An MF model is proposed in [6] and [7] to reduce the number of unknowns and speed up simulation times in comparison with the FE-solution [4]–[7]. Using this approach, the magnetic flux density distribution is approximated by (5) using a truncated Fourier cosine series with N_b terms [7]. Similarly, the magnetic field strength is approximated by (6), where $H_\mathrm{s}(t)$ is the field strength at the surface of the lamination, and function $\beta_\mathrm{n}(z)$ is defined to fulfill $\beta_\mathrm{n}(\pm d/2) = 0$ and $\alpha_\mathrm{n}(z) = -d^2\partial^2\beta_\mathrm{n}(z)/\partial z^2$ [7]

$$B(z,t) = \sum_{\mathrm{n}=0}^{N_\mathrm{b}-1} B_\mathrm{n}(t)\alpha_\mathrm{n}(z); \quad \alpha_\mathrm{n}(z) = \cos\left(2n\pi\frac{z}{d}\right) \tag{5}$$

$$H_\mathrm{appr}(z,t) = H_\mathrm{s}(t) - \sigma d^2 \sum_{\mathrm{n}=0}^{N_\mathrm{b}-1} \frac{\partial B_\mathrm{n}(t)}{\partial t}\beta_\mathrm{n}(z). \tag{6}$$

Weakly satisfying the approximation error between $H_\mathrm{appr}(z,t)$ and the actual field strength $H(z,t)$ yields the following equation system for the magnetic field strength at the surface:

$$\begin{bmatrix} H_\mathrm{s}(t) \\ 0 \\ \vdots \end{bmatrix} = \frac{1}{d}\int_{-d/2}^{d/2} \mathbf{H}(z,t) \begin{bmatrix} \alpha_0(z) \\ \alpha_1(z) \\ \vdots \end{bmatrix} \mathrm{d}z + \sigma d^2 \mathbf{C} \frac{\partial}{\partial t} \begin{bmatrix} B_0(t) \\ B_1(t) \\ \vdots \end{bmatrix}. \tag{7}$$

The elements of matrix $\mathbf{C}$ are found integrating over the lamination thickness [7]. Space integration in (7) can be performed analytically since cosine basis functions are used.

C. Magnetic Equivalent Circuits

The basic model structure forming the backbone for MEC-based models uses the concept of a flux tube, being defined as a tube in which the magnetic fields are invariant in space. Based on the geometries of N flux tubes that discretize the SMSS, a network can be built [4]. Two MECs can be obtained depending on the assumption of possible eddy-current paths. Traditionally, the eddy current i_en is assumed to flow at the inner borders of the flux tube n. This results in a network called $\mathrm{MEC}_{\mathrm{N}-1}$ that can be expressed using (8), shown below, where $i = [1, N]$, l_m is magnetic path length, a is the width of the SMSS, and G_e is the electrical conductivity of the flux tubes

$$H_\mathrm{i}(B_\mathrm{i}) l_\mathrm{m} = n_\mathrm{p} i_\mathrm{p} + \sum_{\mathrm{n}=1}^{i-1} i_\mathrm{en} \tag{8a}$$

$$i_\mathrm{en} = -G_\mathrm{e} \sum_{k=n+1}^{N} \frac{\mathrm{d}\Phi_k}{\mathrm{d}t} = \frac{\sigma d l_\mathrm{m}}{2a} \sum_{k=n+1}^{N} A_{\mathrm{Fe}k} \frac{\mathrm{d}B_k}{\mathrm{d}t}. \tag{8b}$$

A slightly different network can be obtained by assuming that the eddy currents are concentrated on the outer borders of flux tubes, here called MEC_N. In this case, the eddy currents in (8a) are summed up from $n = 1$ to $n = i$, whereas the magnetic flux variations in (8b) are summed up from $k = n$ to $k = N$ due to the fact that one additional eddy-current path is included. However, it is worthwhile to note that both the MEC models represent only a rough approximation, as concentrated eddy currents are assumed. This oversimplification is troublesome, especially when low number of flux tubes N is used.

D. Parametric Magneto-Dynamic Model

The PMD model is in contrast to the MEC models based on the average values of the magnetic variables inside the individual slices (flux tubes) of the SMSS. The advantage of the PMD model is that it takes into account the distribution of the induced eddy currents inside all the slices and their influence on the excitation of magnetic field inside the SMSS [8], [9]. The PMD is expressed by (9), where $\boldsymbol{\Theta}$ represents a vector of the magneto-motive forces generated by the applied current i_p in the excitation winding, $\bar{\mathbf{H}}(\bar{\boldsymbol{\Phi}})$ is a vector of average

magnetic field strengths as the hysteretic functions of the average magnetic fluxes in the slices, and $\mathbf{N}$ is a vector with the number of turns n_p of the excitation winding [8], [9]

$$\boldsymbol{\Theta} = \mathbf{N}i_\mathrm{p} = \bar{\mathbf{H}}(\bar{\boldsymbol{\Phi}})l_\mathrm{m} + \mathbf{L}_\mathrm{m}\frac{\mathrm{d}\bar{\boldsymbol{\Phi}}}{\mathrm{d}t}. \tag{9}$$

The matrix of magnetic inductance $\mathbf{L}_\mathrm{m}$ depends only on the geometric, material properties and on the discretization of the observed SMSS, i.e., the number of slices N.

III. Results

Discussed models were implemented, evaluated, and compared using the software package MATLAB/Simulink. Nonlinear properties related to the local magnetic field strength H_i and magnetic flux densities B_i were taken into account using the inverse ODE Jiles–Atherton hysteresis model [10]. Keeping the mixed form of proposed models, instead of using the differential magnetic permeability, the obtained systems of ODEs can be directly integrated using the backward differentiation formula or Gear's method.

The obtained stiff ODE systems were solved using an implicit Runge–Kutta formula with a first stage that is a trapezoidal rule step and a second stage that is a backward differentiation formula of order two (ode23tb). Model results were validated using measured voltages and currents as model inputs. The PMD model was used as a reference since it was validated for the studied M400-50A NO steel in [8] and [9].

During the first evaluation step, the influence of the discretization of the discussed models was analyzed. A brief summary of the extensive numerical simulations is shown in Fig. 1, where the predicted dynamic loops for maximum flux densities of $B_\mathrm{max} = 1.4$ T at frequency $f = 1000$ Hz for all discussed models were compared for sparse discretization [$N = 5$; see row (a) in Fig. 1] and denser discretization [$N = 20$; see row (b) in Fig. 1]. MEC and FD models were significantly more sensitive to discretization as opposed to the MF and PMD models. Both the MEC-based models failed to correctly predict the dynamic loops at sparse discretization [see column (1) in Fig. 1]. $\mathrm{MEC_{N-1}}$ predicted loops that are too narrow, which is logical as the eddy-current in the outer flux tube was neglected. $\mathrm{MEC_N}$ predicted loops are too wide; hence, the eddy current in the first flux tube flowed only on the surface of the SMSS. Both the observed deficiencies were a direct consequence of too-simplistic assumptions when solving the discussed penetration equation. The error caused by the simplification can be reduced by increasing the density of the discretization, as shown in Fig. 1(b). The deficiencies of the MEC-based models can be eliminated using the PMD model, where the distribution of eddy currents inside individual flux tubes is also taken into account. The obtained results show that, consequently, the PMD model is much more independent of discretization and gives the correct results at much sparser discretization, where the minimum discretization density is correlated with the penetration depth. MEC models converged to the prediction of the PMD model when the discretization density was increased.

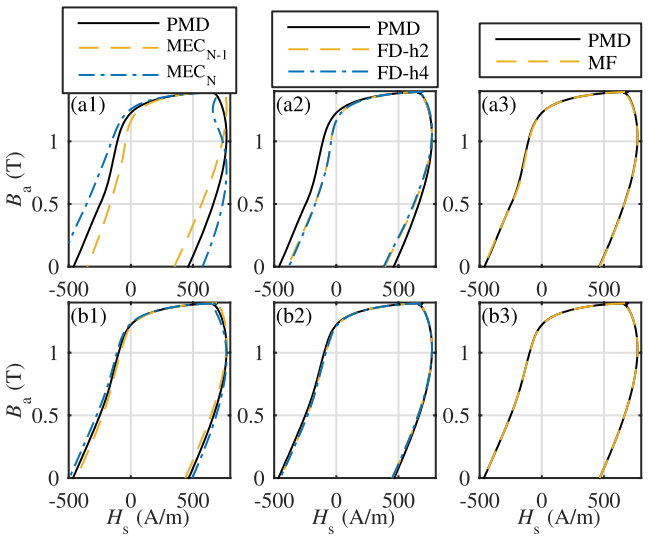

Fig. 1. Dynamic loops for maximum flux densities of 1.4 T at frequency $f = 1000$ Hz for sparse discretization [$N = 5$, row (a)] and denser discretization [$N = 20$, row (b)].

Similar results were obtained for both the FD models [see column (2) in Fig. 1]. When the used discretization density was too small, both the FD models predicted too narrow dynamic loops. The predictions of the FD models also converged to the predictions of the PMD model when increasing the density of discretization, where the convergence was a little faster compared with the MEC models. It was discovered that a minimum of three nodes per penetration depth should be used in the FD models to obtain satisfactory results. In contrast to the MEC and FD models, the predictions of the MF model agreed very well with the PMD model regardless of discretization, where the minimum discretization when applying the cosine transforms to the MF model was also correlated with the skin depth [see column (3) in Fig. 1].

The performed numerical analysis showed that when using high discretization densities ($N \to \infty$), all the discussed models converged to the same result. In order to support the presented findings, the PMD model at high discretization density ($N = 40$) was chosen as the reference model, where the root mean square (RMS) deviations of other model's dynamic loops were analyzed at different discretization densities. The obtained results for maximum flux densities $B_\mathrm{max} = 0.9$ T and $B_\mathrm{max} = 1.4$ T are shown in Fig. 2(a) and (b), respectively. The results support the severe influence of discretization on the MEC and FD-based models. In contrast to this, both the MF and PMD model predictions changed only slightly; when increasing the discretization density 20 times, the RMS deviation was $<1\%$.

Last, all models were analyzed in terms of computational performance. Following the MATLAB recommendations for evaluating the computational performance, three characteristic parameters were evaluated: 1) computation time t_c [s]; 2) number of computed time steps n_ts; and 3) average time to compute one time step $t_\mathrm{c,a}$ [ms]. The results for both voltage- and current-driven versions for maximum flux densities of $B_\mathrm{max} = 1.4$ T at frequency $f = 1000$ Hz are collected in Fig. 3, where the first column corresponds to the voltage-driven versions and the second column to

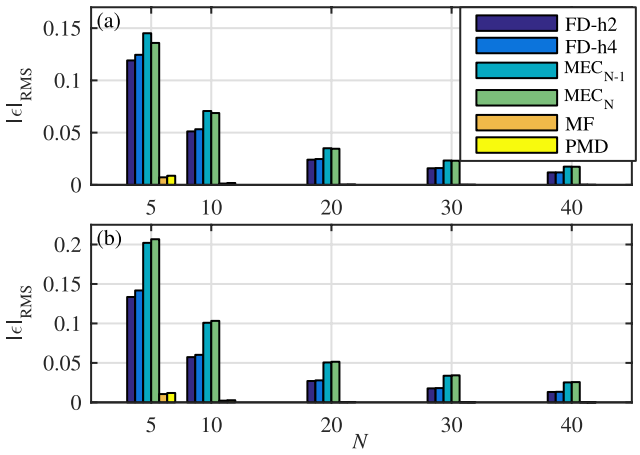

Fig. 2. RMS deviations of other models' dynamic loops at different discretization densities for maximum flux densities. (a) $B_{\max} = 0.9$ T. (b) $B_{\max} = 1.4$ T.

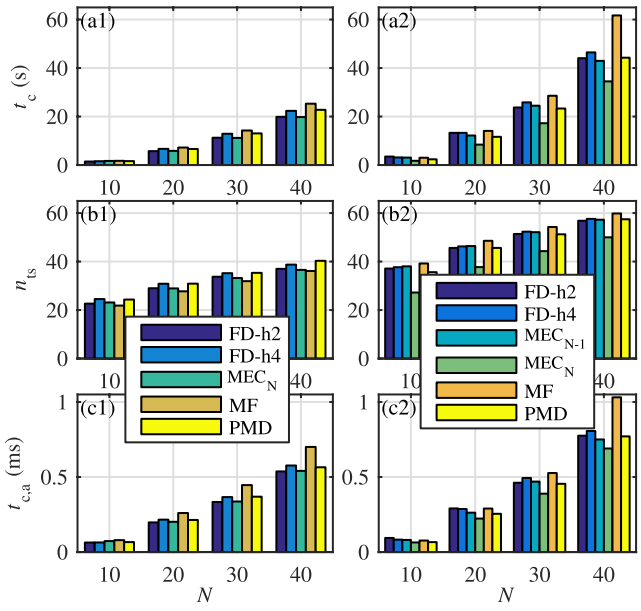

Fig. 3. Computation time t_c [s], number of computed time steps n_{ts}, and average time to compute one time step $t_{c,a}$ [ms] for voltage- [column (1)] and current-driven [column (2)] simulations at $B_{\max} = 1.4$ T.

the current-driven versions. It is worthwhile noting that the voltage-driven version of the $\mathrm{MEC_{N-1}}$ model could not be implemented. In general, the simpler models (FD and MEC models, which have sparse system matrices) required less computational effort. However, the current-driven $\mathrm{MEC_{N-1}}$ and FD model versions required the use of a direct hysteresis model for the surface node/flux tube, which increases the computation times. This is significant, especially at low discretization densities. In contrast to this, the MF and PMD models have much harder coupling between individual regions in the SMSS (hence, denser system matrices) and, thus, required a little more computational effort for the same discretization. The highest computational effort for the same discretization was needed when using the MF model due to the additional cosine transformations. However, when observing the computational performances at the same accuracy, the PMD and MF models outperformed the MEC and FD models by a wide margin due to the high discretization density needed by the latter models. Furthermore, when comparing the PMD and MF models, the PMD model outperformed the MF model due to additional cosine transformations that were performed in the MF model.

IV. Conclusion

In this paper, different 1-D models of SMSSs were analyzed in terms of mathematical structure, implementation work, spatial discretization, accuracy, and computational performance. The obtained results show that the predictions of all the models converged to the same result when the discretization density was increased, where the MF and PMD models stood out in terms of the minimum required discretization density. It is worthwhile noting that in contrast to all other discussed models, both the MF and PMD models can be used for one flux tube/term, where both the models give the classical low-frequency eddy-current approximation. The MF and PMD models are also effortless to implement and flexible, as both the current- and voltage-driven versions can be expressed as simple ODE systems. In terms of computational performance, the PMD model outperforms all the other models.

Acknowledgment

The work of M. Petrun and D. Dolinar was supported by Slovenian Research Agency, under Project P2 0115, Project L2 5489, and Project L2 4114. The work of S. Steentjes was supported by German Research Foundation (DFG) and was carried out under the research project "Improved Modeling and Characterization of Ferromagnetic Materials and their Losses."

References

[1] K. Zakrzewski and F. Pietras, "Method of calculating the electromagnetic field and power losses in ferromagnetic materials, taking into account magnetic hysteresis," *Proc. Inst. Elect. Eng.*, vol. 118, no. 11, pp. 1679–1685, Nov. 1971.

[2] S. E. Zirka, Y. I. Moroz, P. Marketos, and A. J. Moses, "Viscosity-based magnetodynamic model of soft magnetic materials," *IEEE Trans. Magn.*, vol. 42, no. 9, pp. 2121–2132, Sep. 2006.

[3] R. Van Keer, L. R. Dupre, J. A. A. Melkebeek, Y. I. Moroz, and S. E. Zirka, "On the evaluation of transients in conducting ferromagnetic cores," in *Scientific Computing in Electrical Engineering*, vol. 18. Berlin, Germany: Springer-Verlag, 2001, pp. 417–424.

[4] O. Bottauscio, A. Manzin, A. Canova, M. Chiampi, G. Gruosso, and M. Repetto, "Field and circuit approaches for diffusion phenomena in magnetic cores," *IEEE Trans. Magn.*, vol. 40, no. 2, pp. 1322–1325, Mar. 2004.

[5] O. Bottauscio, M. Chiampi, and D. Chiarabaglio, "Advanced model of laminated magnetic cores for two-dimensional field analysis," *IEEE Trans. Magn.*, vol. 36, no. 3, pp. 561–573, May 2000.

[6] J. Gyselinck, R. V. Sabariego, and P. Dular, "A nonlinear time-domain homogenization technique for laminated iron cores in three-dimensional finite-element models," *IEEE Trans. Magn.*, vol. 42, no. 4, pp. 763–766, Apr. 2006.

[7] P. Rasilo, E. Dlala, K. Fonteyn, J. Pippuri, A. Belahcen, and A. Arkkio, "Model of laminated ferromagnetic cores for loss prediction in electrical machines," *Electr. Power Appl.*, vol. 5, no. 7, pp. 580–588, Aug. 2011.

[8] M. Petrun, V. Podlogar, S. Steentjes, K. Hameyer, and D. Dolinar, "A parametric magneto-dynamic model of soft magnetic steel sheets," *IEEE Trans. Magn.*, vol. 50, no. 4, Apr. 2014, Art. ID 7300304.

[9] M. Petrun, V. Podlogar, S. Steentjes, K. Hameyer, and D. Dolinar, "Power loss calculation using the parametric magneto-dynamic model of soft magnetic steel sheets," *IEEE Trans. Magn.*, vol. 50, no. 11, Nov. 2014, Art. ID 6301304.

[10] K. Dezelak, M. Petrun, B. Klopcic, D. Dolinar, and G. Stumberger, "Usage of a simplified and Jiles–Atherton model when accounting for the hysteresis losses within a welding transformer," *IEEE Trans. Magn.*, vol. 50, no. 4, Apr. 2014, Art. ID 7300404.